# Optimizing Interface Conductivity in Electronics

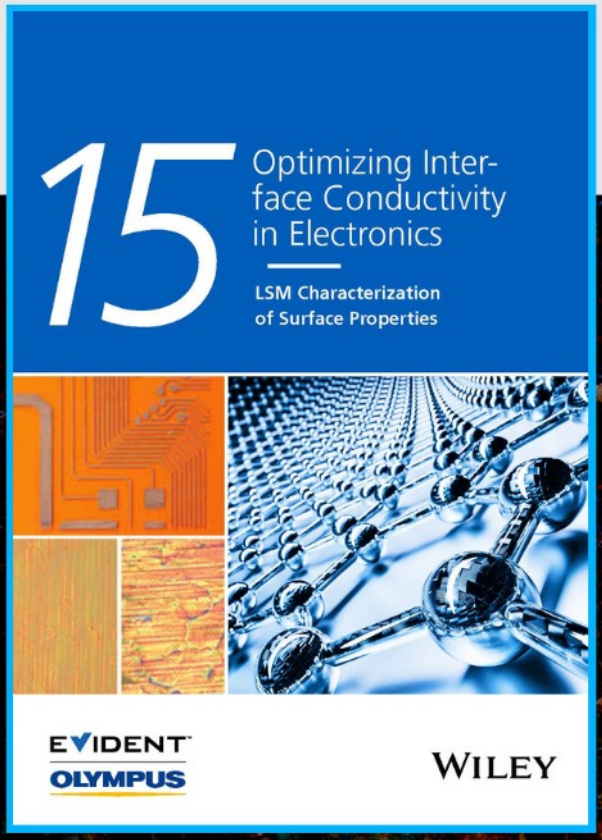


**The latest eBook from Advanced Optical Metrology. Download for free.**

Surface roughness is a key parameter for judging the performance of a given material's surface quality for its electronic application. A powerful tool to measure surface roughness is 3D laser scanning confocal microscopy (LSM), which will allow you to assess roughness and compare production and finishing methods, and improve these methods based on mathematical models.

Focus on creating high-conductivity electronic devices with minimal power loss using laser scanning microscopy is an effective tool to discern a variety of roughness parameters.

EVIDENT
OLYMPUS

WILEY

Check for updates



ADVANCED FUNCTIONAL MATERIALS
www.afm-journal.de

# Highly Tuneable Photochromic Sodalites for Dosimetry, Security Marking and Imaging

*Hannah Charlotte Byron, Claudia Swain, Pyry Paturi, Pauline Colinet, Raphaël Rullan, Vesa Halava, Tangui Le Bahers,* and Mika Lastusaari**

**Photochromic sodalites are considered for a plethora of possible applications, such as UV indexing and X-ray imaging, but for many of these the materials are yet to be optimized. UV indexing can be improved through incremental adjustment of the activation energy of coloration from 300 to 410 nm through replacement of sulfur with selenium. By combining this and other methods of tuning presented in the literature, the excitation threshold and photochromism color can be tuned independently of one another. The range of possible absorption maxima is expanded to 420–680 nm, or almost the entire visible spectrum. Mixing low-cost and easy-to-synthesize sodalites further broadens the possible range of colors and facilitates development of a unique sodalite mix capable of quantifying the doses of two types of UV radiation simultaneously. Finally, the response to X-rays of these highly tuned sodalites is investigated, and it is found that they can be sensitized to produce clear, high-contrast X-ray images at significantly lower doses of radiation than those required by classic photochromic sodalite, $Na_8(AlSiO_4)_6(Cl,S)_2$.**

## 1. Introduction

A photochromic material is one whose color changes when exposed to light. Such a material can be organic or inorganic, with some of the most famous and widely studied examples including azobenzenes, spiropyrans, silver salts and nanoparticles, and tungsten oxides.[1–11] Organic photochromes, sometimes called molecular switches for their ability to switch from one state to another, are highly tuneable, and a broad range of colors is available.[4,5,12] The color changes available from inorganic photochromic materials are more limited, though their temperature and moisture resistance, as well as general durability, is advantageous. Moreover, the library of available colors is growing, and some materials, like polycrystalline $V_2O_5$, have even been shown to change color on exposure to visible light.[13] The majority of photochromic binary transition metal oxides change from a pale yellow-brown to deep blue-black, the result of photoreduction or photo-oxidation followed by a charge transfer.[10,14–18] Metastable F-center formation in vacancies is also a common mechanism for inorganic photochromic materials, and such systems are present in a range of rare-earth activated materials capable of changing

H. C. Byron, C. Swain, M. Lastusaari
Department of Chemistry
University of Turku
Turku FI-20014, Finland
E-mail: miklas@utu.fi

H. C. Byron
Doctoral Programme in Exact Sciences (EXACTUS)
University of Turku Graduate School (UTUGS)
FI-Turku 20014, Finland

C. Swain
Department of Chemistry
University of Durham
Durham DH1 3LE, UK

P. Paturi, V. Halava
Department of Mathematics and Statistics
University of Turku
Turku FI-20014, Finland

P. Colinet, R. Rullan, T. Le Bahers
ENSL
CNRS
UCBL
Laboratoire de Chimie
UMR 5182, 46 allée d'Italie, Lyon69634, France
E-mail: tangui.le_bahers@ens-lyon.fr

T. Le Bahers
Institut Universitaire de France
5 rue Descartes, Paris 75005, France

The ORCID identification number(s) for the author(s) of this article can be found under https://doi.org/10.1002/adfm.202303398

© 2023 The Authors. Advanced Functional Materials published by Wiley-VCH GmbH. This is an open access article under the terms of the Creative Commons Attribution License, which permits use, distribution and reproduction in any medium, provided the original work is properly cited.

**DOI: 10.1002/adfm.202303398**

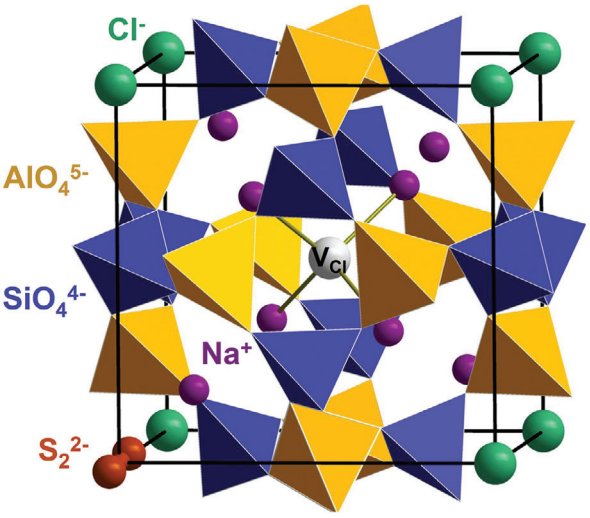


**Figure 1.** Unit cell of photochromic sodalite. One chloride is replaced by the disulfide $S_2^{2-}$ activator responsible for photochromism. A white sphere in the center of the cage corresponds to the chloride vacancy, $V_{Cl}$.

from white to purple, blue, green and yellow.[19–26] The F-center-vacancy mechanism is also found in natural photochromic minerals such as hackmanite, tugtupite and scapolite,[27–29] which are aluminosilicates mostly used for decorative purposes, but which in recent years have sparked interest for a plethora of potential applications.

Synthetic hackmanite, now no longer classed as a mineral itself but as a variety of sodalite,[30] has been studied by scientists since the 1950s.[31–33] Initial studies looked into the reasons behind the photochromism (also called tenebrescence in minerals),[32,34] but in the late 20th century cathodochromic sodalites for data storage applications were of more interest.[35–39] Only since the 2010s has photochromic sodalite been deeply studied with the aim of developing it for commercial applications.[40–44] Its attractive luminescence properties, studied in depth by Norrbo et al., show great potential for use in diagnostic tests, energy storage and safety lighting,[40,45] while the photochromism can be exploited in UV and X-ray dosimetry applications and as passive detectors of high-energy radiation.[41–43] The desired color change of white to pink, purple, blue or yellow can be easily chosen by simple adjustment of the formula and salts used during synthesis.[34,35,37,46] Moreover, all of this is possible without the need for toxic, expensive or rare elements. All of these set photochromic sodalite aside as a uniquely tuneable, low-cost, robust and green inorganic photochromic material. **Figure 1** shows the crystal structure of photochromic sodalite, which has a unit cell parameter of 8.89 Å and belongs to the space group P43n.[45]

In this work, we demonstrate the true versatility of sodalites as inorganic photochromes by presenting the full range of colors available. To the best of our knowledge, no other inorganic material can be tuned to show such a diverse range of photochromic colors through simple adjustments to the formula and stoichiometry. Nevertheless, it is not possible to tune sodalites to change from white to absolutely every possible color: for example, white-to-green photochromism would require absorption in both the blue and red regions of the visible spectrum, which is only possible with two absorption bands. While photochromic sodalites with two different F-centers with different absorption spectra are known, tuning the absorption energy of one without the other is highly challenging.[46] However, we show that this problem is easily mitigated by treating photochromic sodalites as photochromic pigments and mixing them such that the result changes from white to any desired color. For example, using this method we were able to develop sodalite mixes which change from white to orange, green and brown, produced from simple inexpensive starting materials.

Photochromic sodalites show excellent coloration under UVC radiation, X-rays and $\gamma$-rays, though to function as detectors for, e.g., solar UV radiation on Earth's surface, the energy at which coloration occurs must be lowered to the UVA region.[47] Norrbo et al. explored the possibility of this, and found that partial substitution of Na with K or Rb was able to somewhat lower the threshold, though the effect was limited by the solubility of the large ions in the lattice. This was also discussed by Agamah et al. in 2020 while explaining how the presence of potassium can improve the afterglow by reducing competition between the tenebrescence and persistent luminescence phenomena.[48] However, as the coloration occurs when an electron is excited from a $S_2^{2-}$ impurity ($\pi^*$ occupied orbital) into a chloride vacancy ($a_1$ unoccupied orbital),[27,49] it is logical to assume that replacement of disulfide with another species with a higher energy occupied orbital would also reduce the excitation energy.[50] The most obvious choice is another dichalcogenide, such as $Se_2^{2-}$ or $Te_2^{2-}$.[50,51] Few studies have been done on photochromic sodalites prepared with selenium and tellurium, though Ballentyne and Bye showed in 1970 that such materials were indeed photochromic and behaved similarly to their disulfide counterparts,[52] and Reinen and Lindner studied the luminescence of $Se_2^-$ and $Te_2^-$ in ultramarines.[53] In this work, we demonstrate that selenium does indeed affect the activation energy of F-center formation in photochromic sodalites, and the ratio of sulfur to selenium used during synthesis can be used to tune this threshold. Such materials can then be mixed with UVC-sensitive photochromic sodalites of a contrasting color to give a product capable of turning from white to one of several colors, depending on the UV excitation wavelength. This kind of mix can be used to qualitatively identify UV radiation of unknown energy and also to measure the dose of both UVA and UVC radiation simultaneously.

Highly tuned photochromic sodalites containing heavy cations and anions also display an improved response to X-rays. The chlorosodalite ($Na_8(AlSiO_4)_6(Cl,S)_2$) tested by Vuori et al. contains only relatively light elements,[42] meaning it will not strongly interact with X-rays, particularly at the energies used for imaging (20–150 keV).[54] By utilizing sodalites made with elements such as bromine, iodine and rubidium, we were able to produce X-ray images with improved contrast and at lower doses than those used by Vuori et al, including of denser subjects. This is yet again proof that by making simple adjustments to the formula, photochromic sodalites can be tuned and optimized to the desired application, without the need for rare or toxic elements.


© 2023 The Authors. Advanced Functional Materials published by Wiley-VCH GmbH

16163028, 0, Downloaded from https://onlinelibrary.wiley.com/doi/10.1002/adfm.202303398 by University of Turku, Wiley Online Library on [26/07/2023]. See the Terms and Conditions (https://onlinelibrary.wiley.com/terms-and-conditions) on Wiley Online Library for rules of use; OA articles are governed by the applicable Creative Commons License

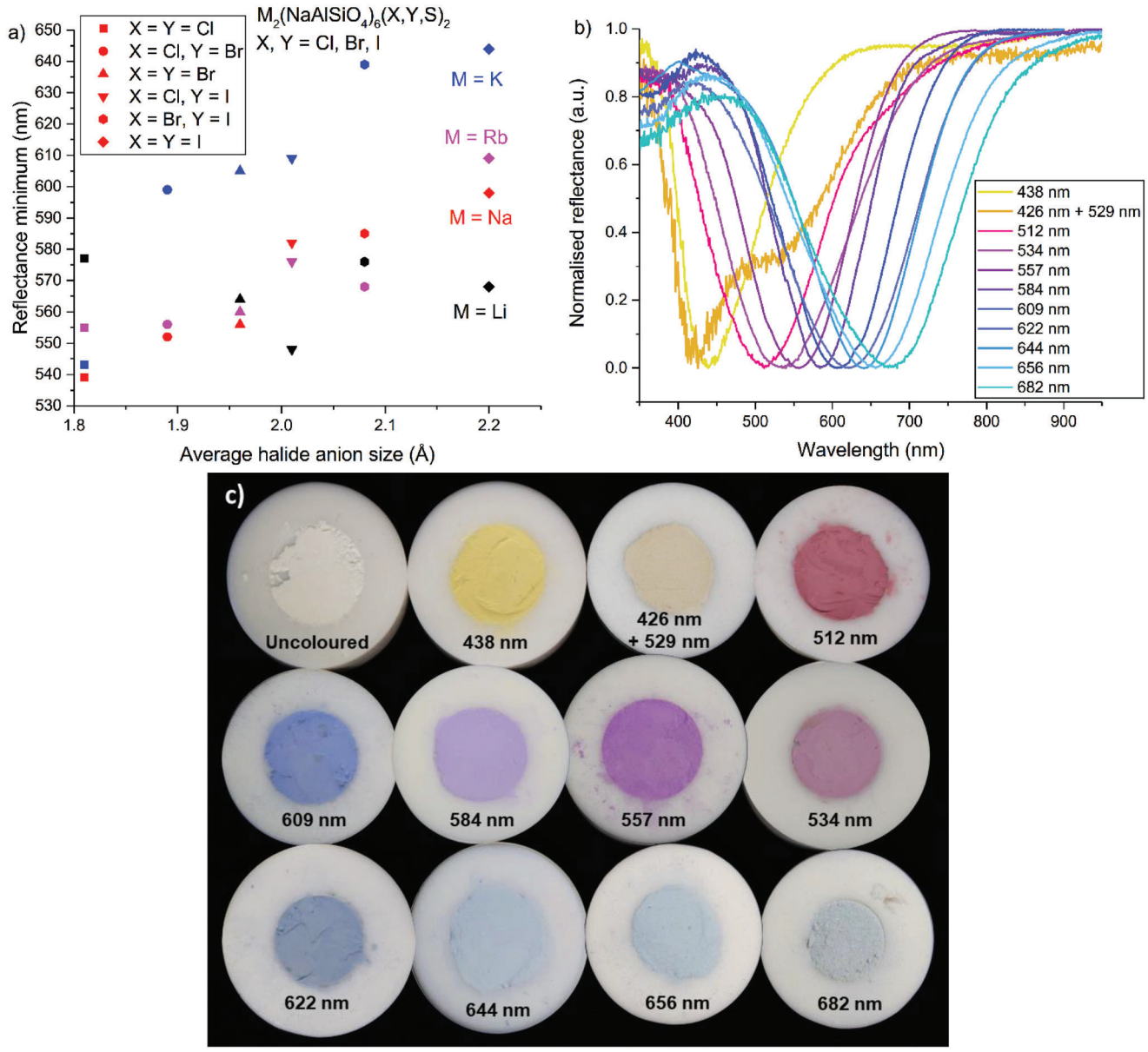


**Figure 2.** a) Effect of different alkali metal cations on the position of the reflectance minimum: the effect of increasingly large average halide anion size is also visible. b) Reflectance curves for photochromic sodalites showing the full range of absorbance maxima achieved thus far. c) Photographs of the colored forms of sodalites in b), including a picture of one uncolored sample. The absorbance maxima of the colored forms are marked next to each sample, and the compositions are given in Table 1.

## 2. Results and Discussion

### 2.1. Full Control of the Photochromism Color

From the literature we know that the tenebrescence color can be changed from pink to purple to blue through substitution of chloride with bromide or iodide, respectively.[35,37,55] This is the result of unit cell expansion increasing the vacancy size and thus shrinking the energy gap between the F-center's HOMO and LUMO.[56] With this aim to tune the HOMO–LUMO bandgap of the F-center, gallium and germanium substitution has also been studied.[9,10] Cation substitution is another way to expand the unit cell: for example, replacing $Na^+$ with $K^+$ or $Rb^+$. To the best of our knowledge, Norrbo et al. are the only group who have studied the photochromism of these types of sodalites, and they did not investigate any changes in absorption spectra at that time.[41] However, our studies show that the cation also has an effect on the position of the absorbance maximum (**Figure 2**a). Colinet proposed through the use of computational studies, that this effect is the result of loss of degeneracy around the F-center, which would lead to broadening of the absorption band due to the presence of multiple possible transitions.[50,51] This appears as a shift in absorption maximum, and band broadening was observed for some materials (Section S1, Supporting Information). However, band


© 2023 The Authors. Advanced Functional Materials published by Wiley-VCH GmbH

16163028, 0, Downloaded from https://onlinelibrary.wiley.com/doi/10.1002/adfm.202303398 by University of Turku, Wiley Online Library on [26/07/2023]. See the Terms and Conditions (https://onlinelibrary.wiley.com/terms-and-conditions) on Wiley Online Library for rules of use; OA articles are governed by the applicable Creative Commons License

**Table 1.** Compositions of the sodalites responsible for the photochromism colors of Figure 2b,c. *Produced by potassium ion exchange of the sodalite with an absorption maxima of 656 nm: exact Na:K ratio is unknown, but it is estimated that 50% of Na was replaced with K[60].

| Position of absorbance maximum [nm] | Composition |
|---|---|
| 438 | $Na_{7.64}Ca_{0.18}(AlSiO_4)_6(Cl,S)_2$ |
| 426 + 529 | $Na_{1.78}Ca_{0.11}(Na,K)_6(AlSiO_4)_6(Cl,S)_2$ |
| 512 | $Na_8(AlSiO_4)_6(Cl,S,Se)_2$; S:Se = 1:1 |
| 534 | $Na_8(AlSiO_4)_6(Cl,S,Se)_2$; S:Se = 2:1 |
| 557 | $Rb_2Na_6(AlSiO_4)_6(Br,S)_2$ |
| 584 | $Na_8(AlSiO_4)_2(Br,I,S)_2$; Br:I = 1:1 |
| 609 | $K_2Na_6(AlSiO_4)_6(Cl,I,S)_2$; Cl:I = 1:1 |
| 622 | $LiNa_6K(AlSiO_4)_6(Br,S)_2$ |
| 644 | $K_2Na_6(AlSiO_4)_6(I,S)_2$ |
| 656 | $K_2Na_6Al_6Si_{4.8}Ge_{1.2}O_{24}(I,S)_2$ |
| 682 | $K_4Na_4Al_6Si_{4.8}Ge_{1.2}O_{24}(I,S)_2$* |

broadening was not significant enough to explain the significant changes in absorption maximum induced by potassium in particular, which we instead believe to be the result of unit cell expansion, or because potassium can be situated further from the center of the cage.[57] Rubidium was found not to induce as great a red-shift in the absorption maximum as potassium, likely due to poor lattice solubility.[41] Likewise a blue-shift in absorption maximum upon lithium substitution was not observed, in part due to lithium sodalites' weak tenebrescence,[40,58] and also because of lithium's tendency to expand the vacancy.[55] Instead, the position of the reflectance minimum for lithium sodalites remained roughly constant, while for other alkali metals the halogen's effect is observable. However, by utilizing the already large red-shift in absorption maximum caused iodine in conjunction with that of potassium, we were able to push the absorption maximum to 650 nm (in comparison with the 540 nm absorption of the pristine sodalite). Furthermore, by combining this with partial substitution of Si with Ge, we were able to extend the range of possible absorption maxima to 680 nm (Figure 2b).

Some of us recently showed how this range of F-center absorption wavelengths can be even further expanded in the other direction by partial substitution of sodium with calcium to raise the energy of the F-center's LUMO.[46] These materials change color from white to yellow, with the exact color being the result of an interplay of pink and yellow F-centers (absorbing 520 and 430 nm respectively). Depending on the ratio of pink- to yellow-absorbing F-centers in the material, the tenebrescence may appear pink, yellow or pale orange. Thus, through simple adjustments of the formula, it is possible to produce photochromic sodalite that changes from white to almost any other color, with an easily tuneable F-center absorption maximum ranging from 420–680 nm, or almost the entire visible spectrum (Figure 2c, **Table 1**). Not only is it possible to tune sodalites to show comparatively unusual color changes (white to yellow, white to orange), but with the exception of the very long wavelengths (650–680 nm), tuning does not require any elements considered rare, according to the ACS periodic table of endangered elements.[59] It should be noted that F-centers can also show luminescence. We recorded the emission spectra for each sample presented in this work (see the Supporting Information) , and observed blue (due to $Ti^{3+}$–$V_O$ pairs) and red ($Fe^{3+}$) emissions typical of sodalites ,[48] but no color center emission was observed.

Despite this greatly increased range of tenebrescence colors, one color remained truly elusive: green. Green light is located in the middle of the electromagnetic spectrum (500–560 nm), so for an object to appear green, it must absorb light at either end of the visible spectrum and reflect the middle portion. This is challenging for photochromic sodalites, which usually possess only one absorption band. While the aforementioned yellow photochromic sodalites do usually contain two types of F-center and thus two absorption bands, separating these bands is challenging: shifting the absorbance of the pink $Na_4$ F-centers using larger halides is impossible without destroying the 430 nm absorption of the $Na_2Ca$ F-centers.[46] A proper orange color has also proved difficult to obtain: Ca-containing sodalites with pink and yellow bands of roughly equal intensity generally show only a weak color change (Figure 2c),[46] and the F-center is yet to be tuned to absorb in a suitable range for a white-to-orange color change (460–490 nm).

In order to overcome these shortcomings, we attempted to mix two or more photochromic sodalites as if they were paint: we now have access to the three primary colors of pigments – pink, yellow and blue – and thus they can be mixed together to produce green, orange or any desired color. Mixing photochromic sodalites is somewhat challenging, as they are all usually white before exposure to UV. When mixing, we started by choosing materials with roughly equally intense absorption bands and mixing them in equal amounts (**Figure 3**a). The resulting color was checked by briefly irradiating with UV, and the composition adjusted if necessary. Through mixing, we have finally completed the collection of possible colors of photochromic sodalites, including all colors of the visible spectrum as well as neutral colors like brown. Interestingly, mixing weakened the overall intensity of the colored form, as is particularly visible for the green mix. This is likely due to a reduced concentration of each type of color center in the overall mix. The L*a*b* coordinates, however, confirm that this material is indeed green in its colored form (Figure 3b). Photographs of the colored forms of these materials are shown in Figure 3c. Note that the orange, green, and brown materials are sodalite mixes; all other colors arise from one pure type of photochromic sodalite.

These mixes are suitable for any applications of photochromic sodalites thus far presented in the literature, such as dosimeters, detectors, and security markers, amongst others.[41–44,61] They present the added advantage of true color customization, and can be produced from cheap precursors: pink sodalite ($Na_8(AlSiO_4)_6(Cl,S)_2$), yellow sodalite ($Na_{7.64}Ca_{0.18}(AlSiO_4)_6(Cl,S)_2$) and blue sodalite ($Na(AlSiO_4)_6(I,S)_2$ or $K_2Na_6(AlSiO_4)_6(Br,S)_2$).

### 2.2. Tuning the Excitation Threshold for Dosimetric Applications

First, we present the results of lowering the activation energy of F-center formation through substitution of sulfur with selenium. TD-DFT analyses predict that both selenium and tellurium will lower the activation energy,[50] and indeed both were tested in this


© 2023 The Authors. Advanced Functional Materials published by Wiley-VCH GmbH

16163028, 0, Downloaded from https://onlinelibrary.wiley.com/doi/10.1002/adfm.202303398 by University of Turku, Wiley Online Library on [26/07/2023]. See the Terms and Conditions (https://onlinelibrary.wiley.com/terms-and-conditions) on Wiley Online Library for rules of use; OA articles are governed by the applicable Creative Commons License

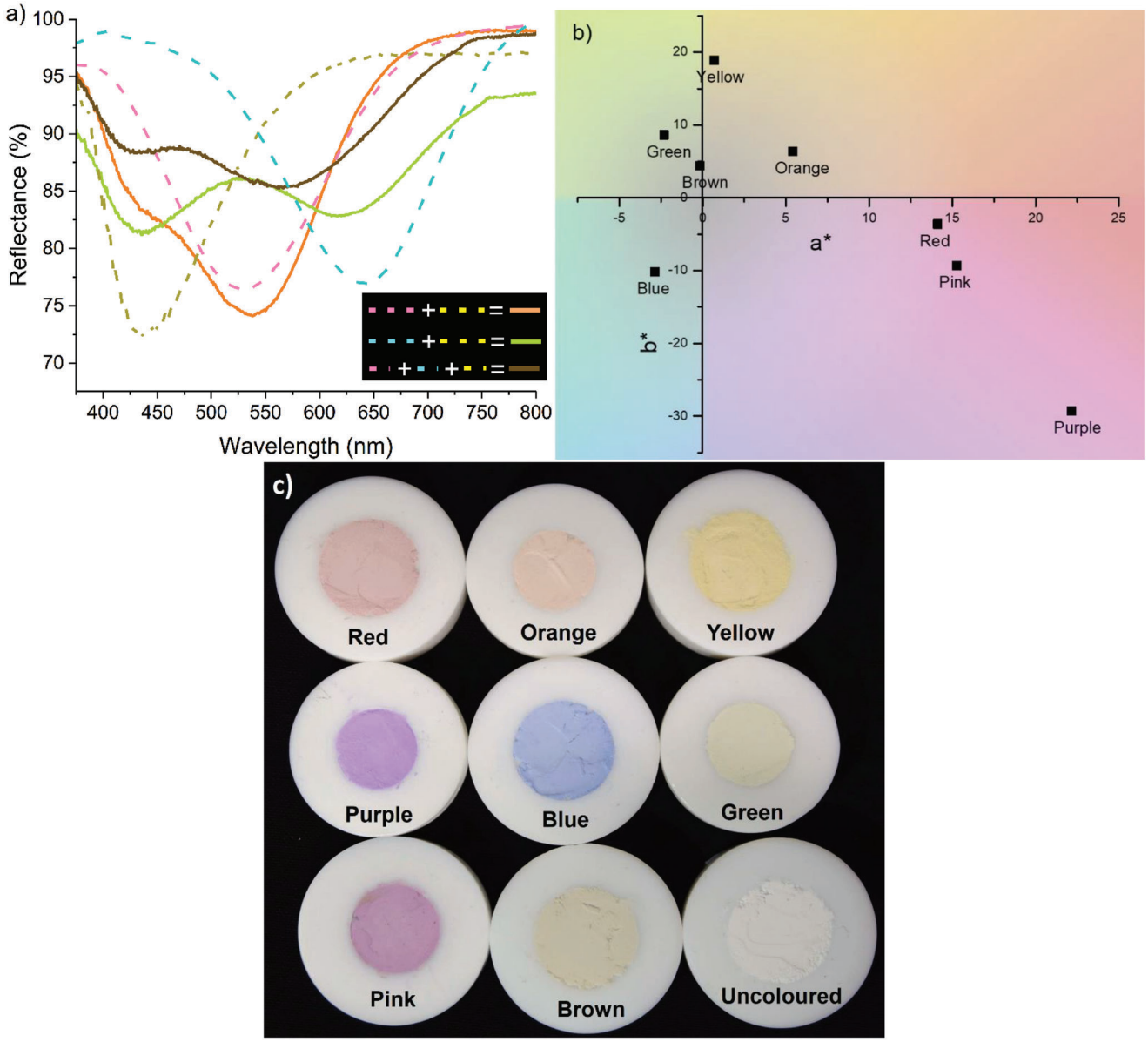


**Figure 3.** a) Reflectance curves of green, orange, and brown mixes in their colored forms, as well as the pink, yellow and blue photochromic sodalites used to produce them. b) a* and b* coordinates of the colored forms of the range colors available. c) Photographs of the range of photochromic sodalites in their colored forms.

way, though all materials made with tellurium were very dark in color, and thus any color change upon exposure to UV was not visible to the eye. The effect of selenium on the excitation spectra of tenebrescence was immediate, with coloration occurring at gradually lower energies as the amount of selenium in the material increases. **Figure 4**a shows the excitation spectra of tenebrescence in selenium-containing photochromic sodalites. Here we see that at 25 mol% selenium substitution there is already an increase in coloration intensity induced by 325 nm radiation. By 50 mol% Se substitution coloration begins at 380 nm and when sulfur is fully replaced by Se, coloration begins at 410 nm. This observation is supported by TD-DFT calculations of system containing an $E_2^{2-}$ (E = S, Se) impurity substituting a $Cl^-$ ion in the vicinity of a $Cl^-$ vacancy. The charge transfer transition corresponding to the $^1[E_2^{2-}(\pi^*),V_{Cl}(a_1)] \rightarrow {}^1[E_2^{-}(\pi^*),V_{Cl}^{-}(a_1)]$ electronic transition is computed at 3.61 eV for $S_2^{2-}$ and 3.33 eV for $Se_2^{2-}$ activators. We further hypothesized the formation of a $SeS^{2-}$ activator for mixed composition materials with a computed charge transfer transition energy at 3.48 eV. In other words, TD-DFT overestimates the transition energies (by ≈0.2–0.3 eV) but reproduces the trend observed experimentally quite well. In term of orbitals involved, the Figure S4 (Supporting Information) shows the HOMO and LUMO orbitals involved in the charge transfer transition where we can see that going from S to Se does not change the chemical nature of the orbitals involved (Section S3, Supporting Information). The position of the


© 2023 The Authors. Advanced Functional Materials published by Wiley-VCH GmbH

16163028, 0, Downloaded from https://onlinelibrary.wiley.com/doi/10.1002/adfm.202303398 by University of Turku, Wiley Online Library on [26/07/2023]. See the Terms and Conditions (https://onlinelibrary.wiley.com/terms-and-conditions) on Wiley Online Library for rules of use; OA articles are governed by the applicable Creative Commons License

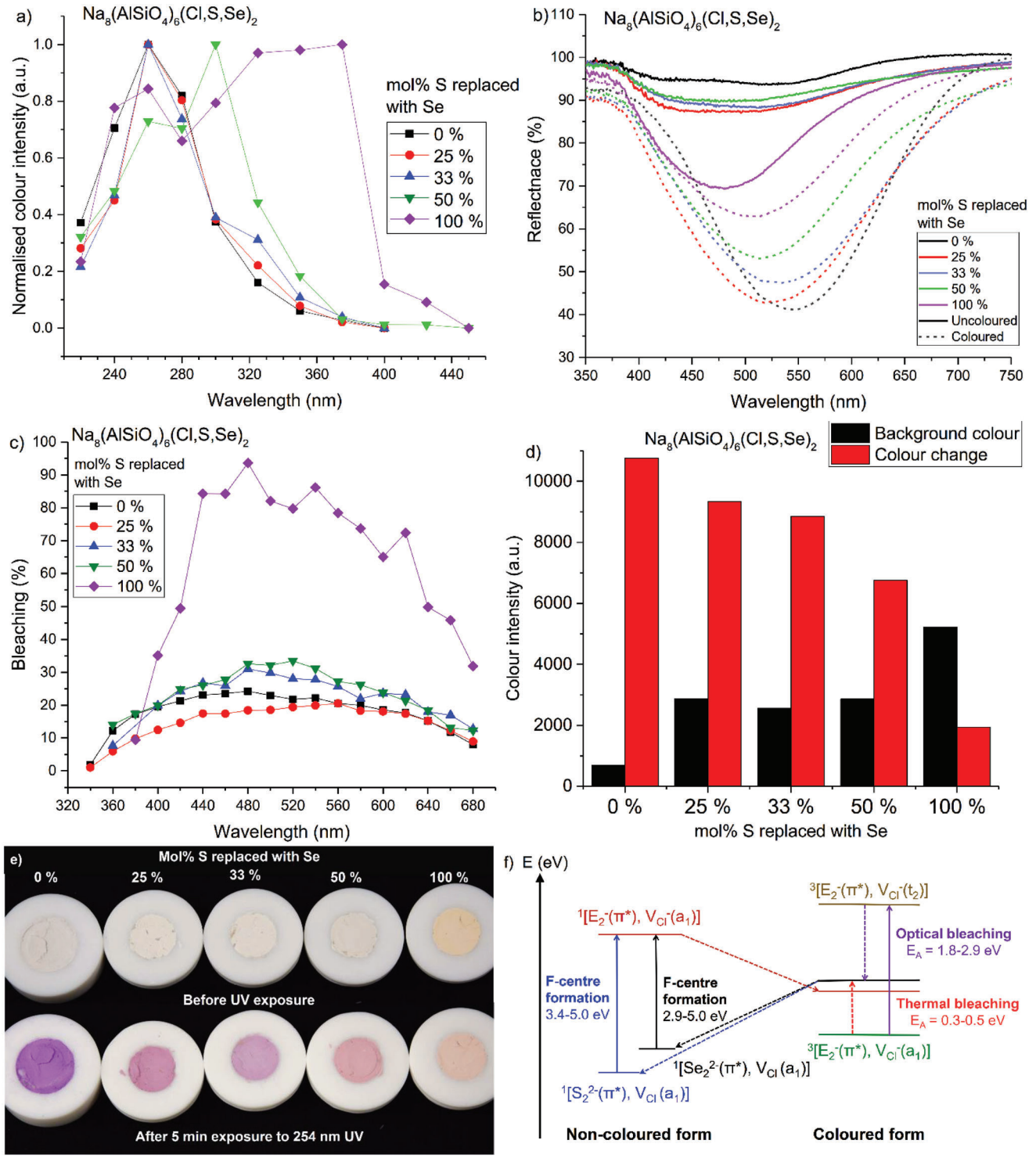


**Figure 4.** a) Tenebrescence excitation spectra of chloride sodalites with selenium replacing 0–100 mol% of sulfur. b) Reflectance spectra of the samples in a) before and after 5 min irradiation with 254 nm UV. The white reference was MgO. c) Optical bleaching spectra corrected for spontaneous fading in darkness. d) Color intensities of the background color and color change after exposure to UV. e) Photos before and after UV irradiation. f) Effect of selenium on the mechanism of F-center formation and thermal and optical bleaching. Electron transfers initiated by photoexcitation are marked with solid arrows, while nonradiative geometrical relaxations are indicated by dotted arrows. As more selenium replaces sulfur, the relative number of $^1[S_2^{2-}(\pi^*), V_{Cl}(a_1)]$ decreases and $^1[Se_2^{2-}(\pi^*), V_{Cl}(a_1)]$ increases. E = S or Se. Figure (f) is adapted from Norrbo et al (2018).[41]


© 2023 The Authors. Advanced Functional Materials published by Wiley-VCH GmbH

16163028, 0, Downloaded from https://onlinelibrary.wiley.com/doi/10.1002/adfm.202303398 by University of Turku, Wiley Online Library on [26/07/2023]. See the Terms and Conditions (https://onlinelibrary.wiley.com/terms-and-conditions) on Wiley Online Library for rules of use; OA articles are governed by the applicable Creative Commons License

**Table 2.** Calculated optical bleaching energies obtained from thermotenebrescence measurements and measured excitation thresholds of F-center formation compared to those predicted by TD-DFT (using $S_2^{2-}$, $SeS^{2-}$, and $Se_2^{2-}$ activators to simulate 0%, 50%, and 100% of S replaced by Se respectively)[64].

| Mol% S replaced with Se | Trap $E_A$ [$\times 10^{-21}$ J] | Trap depth [eV] | Excitation threshold [eV] | Excitation threshold predicted by TD-DFT [eV] |
|---|---|---|---|---|
| 0% | $76 \pm 3$ | $0.47 \pm 0.02$ | 3.44 | 3.61 |
| 25% | $49 \pm 2$ | $0.31 \pm 0.01$ | 3.44 | – |
| 33% | $46 \pm 3$ | $0.29 \pm 0.02$ | 3.44 | – |
| 50% | $49 \pm 5$ | $0.31 \pm 0.03$ | 3.26 | 3.48 |
| 100% | $48 \pm 3$ | $0.30 \pm 0.02$ | 3.02 | 3.33 |

reflectance minimum does not significantly change with increasing amounts of selenium, suggesting it does not affect the vacancy size considerably and thus the absorption energies of the F-center formed on UV excitation (Figure 4b). The bleaching spectra of these materials are as expected, i.e., optimal bleaching occurs at the same wavelengths we observe maximum absorbance of the F-center (440–620 nm, maximum ≈500 nm, Figure 4c), again supporting the theory that selenium does not affect the energy levels of the F-center. The sample containing only Se has a noticeably narrower optical bleaching band, due to its low coloration threshold. This material also bleaches significantly more easily than those containing some sulfur, likely because the relative color change is small, hence the relative bleaching percentage is much larger for this sample.

The selenium-containing materials also generally have stronger body colors, i.e., their permanent color is a pale orange even before exposure to UV (Figure 4e). To identify the reason for this, Raman spectroscopy was performed to investigate the presence of radical anions such as $S_2^-$, $S_3^-$, and $Se_2^-$, which may be responsible for the color (Section S2, Supporting Information). By comparing the Raman spectra to the reflectance spectra of uncolored chlorosodalites with differing S:Se and the literature, it was concluded that the darkening body color was the result of $Se_2^-$ species, as in red ultramarines.[53,62,63] This is further supported by the TD-DFT simulated absorption wavelength of a $Se_2^-$ trapped in a sodalite computed at 460 nm.[56] Increasing the amount of selenium increases the proportions of $Se_2^-$ in the material, which is believed not to participate in photochromism. This explains the gradually weakening photochromic response seen in Figure 4b,d – there is a gradually decreasing concentration of the $S_2^{2-}$ and $Se_2^{2-}$ activators required for photochromism. XRF measurements taken after washing also confirm the presence of selenium in the structure, despite concerns that the $Na_2SeO_3$ starting material would decompose during synthesis (Section S2, Supporting Information). These materials also retain the blue-white photoluminescence and persistent luminescence properties of synthetic photochromic sodalites (Section S2, Supporting Information).[49] The observed effects of gradual sulfur substitution with selenium on the body color and excitation spectra also holds true for other sodalite compositions (Section S4, Supporting Information).

Thermotenebrescence[41] fade curves of selenium and sulfur-selenium sodalites were measured to investigate selenium's effect on the thermal bleaching energy. Contrary to expectation, the thermal bleaching energy did not gradually decrease with selenium content. Instead, the thermal bleaching energy dropped immediately from 0.47 eV to 0.30 eV with introduction of only 25 mol% Se and remained the same for all subsequent samples (**Table 2**). The sudden change suggests that introduction of even a small amount of Se destabilizes the F-center similarly to potassium, which lowers the activation energy of thermal bleaching.[51] Indeed, the obtained trap depth is close to that reported for $(Na,K)_8(AlSiO_4)_6(Cl,S)_2$ (0.28 eV).[41] On the other hand, the gradual decrease in F-center activation energy with increasing selenium content can be explained by the increase in energy of the HOMO of the activator when going from S to Se (Figure 4f).

### 2.3. Simultaneous Passive Dosimetry of UVA and UVC Radiation

The ability to finely tune the excitation threshold through introduction of selenium improves photochromic sodalite's prospects for UV indexing and dosimetry, as it can be easily and reliably sensitized to UVB and UVA radiation. In Section 2.1, two or more sodalites excitable by UVC were mixed to produce any desired tenebrescence color. Following from this, we considered the idea of mixing two photochromic sodalites with differing excitation spectra and contrasting colors to develop a passive radiation indicator. Such a mix would change from white to one of two colors, depending on the wavelength of UV it was exposed to. The color intensity would also give an indication of the dose, further expanding the functionality of such a material as a passive multifunctional detector.

A range of photochromic sodalite mixes were developed with the aim of achieving distinctly different colors when the mix was excited with UVA or UVC. **Figure 5**a shows an example of how such a mix is chosen: the reflectance curves of the colored forms of the two components used, along with their excitation spectra, are good indicators of whether a mix will work. Ideally the two components are excited by different wavelengths of UV, and their absorbance maxima are distinctly separate too. In this example, we considered one blue iodosodalite and one pink chlorosodalite made with selenium. While both are excited by UVC, the difference in coloration intensities will cause the blue sodalite to dominate under excitation by 280 nm and below, while above 320 nm only the pink sodalite is excited. This is demonstrated in Figure 5b, where the change in reflectance minimum with respect to excitation wavelength of a similar mix is clearly visible. The variation is around 50 nm, the material appearing blue-violet under UVC radiation, violet under UVB and pink under UVA. This mix was


© 2023 The Authors. Advanced Functional Materials published by Wiley-VCH GmbH

16163028, 0, Downloaded from https://onlinelibrary.wiley.com/doi/10.1002/adfm.202303398 by University of Turku, Wiley Online Library on [26/07/2023]. See the Terms and Conditions (https://onlinelibrary.wiley.com/terms-and-conditions) on Wiley Online Library for rules of use; OA articles are governed by the applicable Creative Commons License

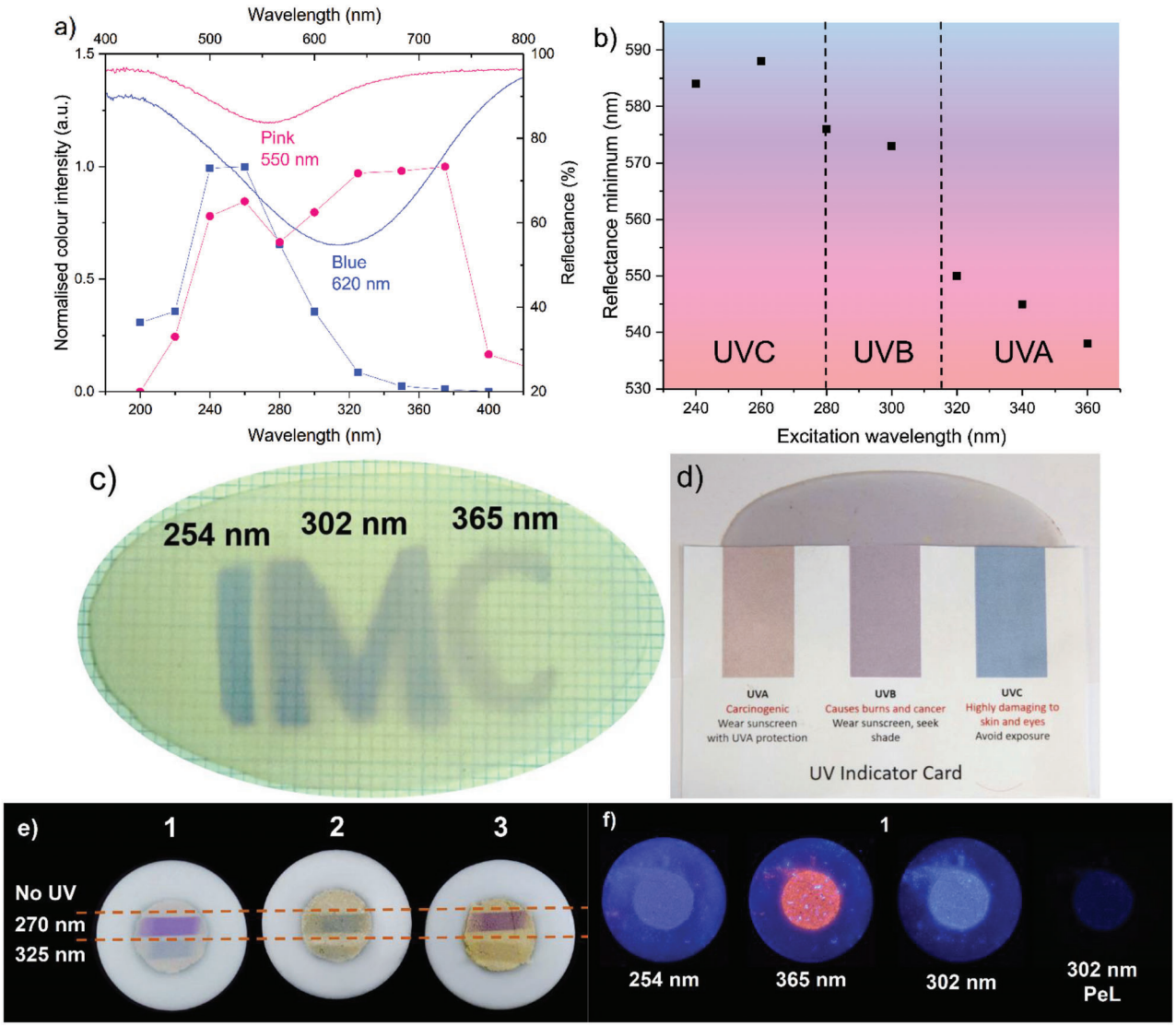


**Figure 5.** a) Tenebrescence excitation spectra and reflection spectra of the colored forms of two sodalites considered for a wavelength-sensitive photochromic mix. b) Change in reflectance minimum for a similar mix to that presented in a) with respect to UV excitation wavelength. c) A film cast from a sodalite mix with "IMC" written on it using three different wavelengths of UV and a stencil. d) Use of the mix in c) for qualitative detection of UVA, UVB, or UVC. e) Examples of other mixes showing different tenebrescence colors under the given UV wavelengths. f) Photo- and persistent luminescence (PeL) of mix **1** from e) under three different UV lamps.

subsequently used to produce a flexible tape, using a modified version of the method presented by Abhinay et al.,[65] and with the aid of a stencil the acronym IMC was made using three different UV wavelengths (Figure 5c). The different colors of the letters are apparent.

This sodalite mix film was then tested as a dosimeter. After calibration of the rise of tenebrescence color excited by UVA and UVC respectively (Section S6, Supporting Information), the tape was colored by two UV sources simultaneously. **Figure 6** shows the results of quantitative dosimetry with this mix, showing the material was able to estimate the dose (fluence) of both UVA and UVC radiation with exposed to them simultaneously (**Table 3**). A detailed discussion of the development and functionality of the model is given in the Supporting Information, though the equations used to describe the relationship between UVA dose (fluence), UVC dose and the measured coloration intensities are given in Equations (1) and (2). In these equations, the terms

**Table 3.** Regression data from linear fitting of the data in Figure 6.

| UV type | UVA | | UVC | |
|---|---|---|---|---|
| Test number | 2 | 6 | 2 | 6 |
| Intercept | −2 ± 3 | 1.4 ± 1.2 | 3 ± 3 | −1.3 ± 0.4 |
| Slope | 1.1 ± 0.3 | 1.2 ± 0.2 | 1.2 ± 0.1 | 1.11 ± 0.05 |
| Residual sum of squares | 187.6 | 26.1 | 162.1 | 3.2 |
| Pearson's *r* | 0.7826 | 0.8718 | 0.9503 | 0.9908 |
| $R^2$ | 0.61246 | 0.76011 | 0.90299 | 0.98178 |


© 2023 The Authors. Advanced Functional Materials published by Wiley-VCH GmbH

16163028, 0, Downloaded from https://onlinelibrary.wiley.com/doi/10.1002/adfm.202303398 by University of Turku, Wiley Online Library on [26/07/2023]. See the Terms and Conditions (https://onlinelibrary.wiley.com/terms-and-conditions) on Wiley Online Library for rules of use; OA articles are governed by the applicable Creative Commons License

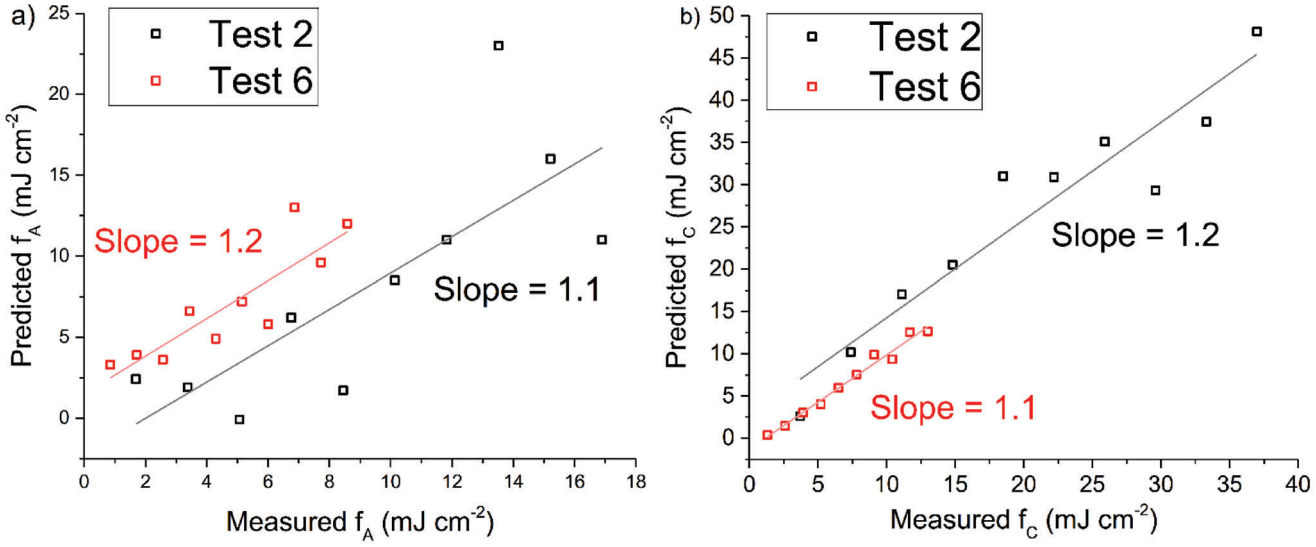


**Figure 6.** Plots showing how well the model was able to predict the fluences of UVA a) and UVC b). A slope of close to 1 indicates good prediction by the model. Full results from fitting of the straight lines are given in **Table 3**.

$y_{0474,A}$, $A_{474,A}$, $R_{0474,A}$, $y_{0474,C}$, $A_{474,C}$, $R_{0474,C}$, $y_{0603,A}$, $A_{603,A}$, $R_{0603,A}$, $y_{0603,C}$, $A_{603,C}$, and $R_{0603,C}$ are all obtained from fitting of calibration data integrated at 474 and 603 nm respectively, $A_{1474,}$ $A_{2474}$, $p_{474}$, $x_{0474}$, $A_{1603,}$ $A_{2603}$, $p_{603}$, and $x_{0603}$ are obtained from fitting a function that relates measured and predicted coloration intensities at 474 and 603 nm respectively, $I_{474}$ and $I_{603}$ are the measured color intensities at 474 and 603 nm, respectively, $f_A$ is the dose of UVA radiation determined by the model and $f_C$ is the dose of UVC radiation determined by the model

$$A_{474,A} \cdot e^{R_{0,474,A} f_A} = A_{1,474} - y_{0,474,A} - y_{0,474,C} + \frac{A_{2,474} - A_{1,474}}{1 + 10^{p_{474}(x_{0,474} - I_{474})}} - A_{474,C} \cdot e^{R_{0,474,C} f_C} \quad (1)$$

$$A_{603,A} \cdot e^{R_{0,603,A} f_A} = A_{1,603} - y_{0,603,A} - y_{0,603,C} + \frac{A_{2,603} - A_{1,603}}{1 + 10^{p_{603}(x_{0,603} - I_{603})}} - A_{603,C} \cdot e^{R_{0,603,C} f_C} \quad (2)$$

This kind of analysis requires an accurate spectrometer capable of measuring the change in reflectance after exposure to UV, and the results were interpreted by solving Equations (1) and (2) numerically. However, it does demonstrate that photochromic sodalite mixes can be used to detect and measure the dose of more than one type of radiation hitting the same spot passively. Such a passive detector would not require any electronics during measurement and can be left in the testing area to measure the dose, which is then determined afterward from the intensity of the color change. This kind of material can also be used more qualitatively, by comparing to a reference card which allows the user to determine which type of radiation they were exposed to (Figure 5d).

Since excitation threshold can be tuned independently to the photochromism color, this kind of detector is not limited to these two colors. Utilizing selenium and potassium's effects on the excitation threshold,[41] we were able to produce several mixes showing different colors under UVC and UVA excitation (Figure 5e). In this figure, mix **1** functions in the opposite way to the mixes in Figure 5a–d : it is pink under UVC and blue under UVA. Mix **2** is blue under UVC and yellow-green under UVA; mix **3** is pink under UVC and yellow under UVA. These mixes also retain all the luminescence properties of their starting materials, which would also render them attractive materials for security marking (Figure 5f).

### 2.4. Use of Heavy Ions to Improve X-Ray Imaging

In 2021, Vuori et al. presented for the first time how photochromic sodalites could be used to make X-ray images.[42] In their work they used unmodified sodalite, i.e., $Na_8(AlSiO_4)_6(Cl,S)_2$. The elements present in this kind of sodalite are some of the lightest in the periodic table, which means their photoelectric absorption coefficients are relatively low.[66] While pushing the limits of the absorption band of photochromic sodalite in Section 2.1 , it occurred to us that some of the heavier elements we used, such as bromine, iodine and potassium, may have helped sensitize these materials to X-rays. We therefore sought to investigate this, to explore how tuning photochromic sodalites can be used to improve their potential for X-ray imaging, particularly focusing on lowering the required dose to produce a clear image.

When photochromic sodalite is exposed to X-rays, color center formation does not occur via a simple electron transfer from a neighboring $S_2^{2-}$ species to an adjacent chlorine vacancy. Instead, a cascade of electrons and holes is created, which eventually relax to form the color center. The full mechanism of photochromic sodalite's coloration under X-rays is explained in detail in Vuori et al.'s 2021 paper.[42] The penetrating nature of X-rays means that upon X-ray exposure, the entire sample changes color,


© 2023 The Authors. Advanced Functional Materials published by Wiley-VCH GmbH

16163028, 0, Downloaded from https://onlinelibrary.wiley.com/doi/10.1002/adfm.202303398 by University of Turku, Wiley Online Library on [26/07/2023]. See the Terms and Conditions (https://onlinelibrary.wiley.com/terms-and-conditions) on Wiley Online Library for rules of use; OA articles are governed by the applicable Creative Commons License

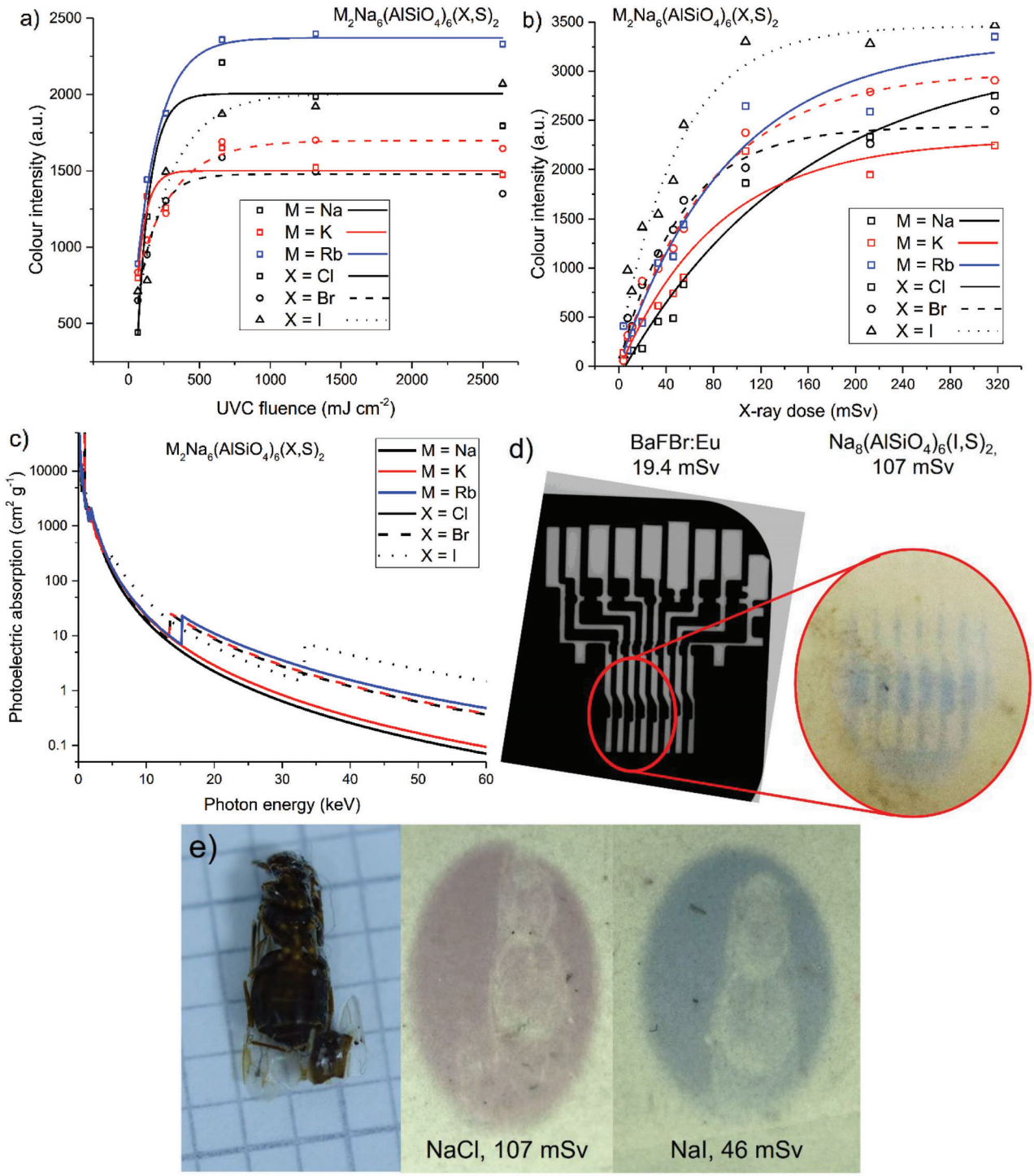


**Figure 7.** a) Coloration intensity with respect to UV dose (fluence) of photochromic sodalites of differing compositions. b) The same materials' dose–response curves when excited with X-rays. c) Photoelectric absorption coefficients for sodalites containing heavy ions.[69] d) X-ray image of the internal electronics of a micro SD adapter taken with a commercial phosphor imaging plate and an iodosodalite tape. e) X-ray images of a flying ant (left) produced on two different photochromic sodalite tapes at different doses. The salt used in sodalite synthesis (MX) is indicated.

rather than just the surface. Thus, the surface coloration intensity induced by X-rays will be weaker than that of UV. Due to this penetration, it is also not possible to directly compare the doses of UV to X-rays. However, when we compare the behavior of different sodalites under UV versus X-rays, we do see the effect of the heavier ions on the material's sensitivity to X-rays. **Figure 7**a shows that the order of color intensities after exposure to UV is somewhat random: M = Rb, X = Cl colors most strongly, and M = Na, X = Br least strongly. However, when we look at the responses under X-ray, we see a much more logical pattern: M = Na,


© 2023 The Authors. Advanced Functional Materials published by Wiley-VCH GmbH

16163028, 0, Downloaded from https://onlinelibrary.wiley.com/doi/10.1002/adfm.202303398 by University of Turku, Wiley Online Library on [26/07/2023]. See the Terms and Conditions (https://onlinelibrary.wiley.com/terms-and-conditions) on Wiley Online Library for rules of use; OA articles are governed by the applicable Creative Commons License

X = I being the best and M = K, X = Cl the worst (Figure 7b). While the characteristic emission of the X-ray source used is 22 keV (silver anode), at 50 kV the bremsstrahlung from such an X-ray tube passes well above the K-edge of iodine (33.2 keV).[67,68] Thus, when we consider the calculated photoelectric absorption coefficients for sodalites of the given compositions (Figure 7c),[69] it is understandable that the materials made with sodium iodide and rubidium chloride perform the best. Bromosodalites generally outperformed their chlorosodalite counterparts, though interestingly, the M = Na, X = Cl sample used in this study colored surprisingly well under X-rays at very high dose (>120 mSv). However, below this dose it colors relatively weakly, as expected. With the aim in mind of reducing the X-ray dose required for clear imaging, the impact of heavier ions on X-ray sensitivity at doses of <100 mSv is clear, regardless of how strongly the sample is able to color under UV.

Figures 7d,e demonstrate how replacing chloride in regular sodalite with iodide improves the material's suitability for X-ray imaging dramatically, both in terms of image contrast and by reducing the required dose. In Figure 7d, the application of quality control of electronic components proposed by Vuori et al. was tested on a micro SD adapter. The image produced with iodosodalite was compared to that produced by a commercial computed radiography (CR) plate (phosphor material: BaFBr:Eu). The dose required by sodalite is significantly higher than that of the CR plate, though this is in part because the majority X-rays produced by our XRF device are relatively soft and likely do not penetrate the SD reader significantly enough to color the sodalite well. Industrial radiography is usually performed using an X-ray tube with a tungsten anode working at ≥100 kV, with a characteristic emission of 57.9 keV.[70–72] These harder X-rays are more suitable for penetrating an inorganic sample and will also be absorbed by the iodosodalite strongly, resulting in a better image (Figure 7c). Furthermore, the iodosodalite film does not need to be kept in the dark before reading, nor is an expensive reader required – the image is immediately visible to the eye and can be recorded with a simple camera.

Soft organic samples are also better imaged with iodosodalite, as shown in Figure 7e. The internal structure of the ant is clearly visible on the iodosodalite tape after exposure to less than half the X-ray dose used to produce an image of similar quality with chlorosodalite. The blue color of iodosodalite also appears darker to the eye, resulting in higher contrast. Theoretically, photochromic sodalite prepared with potassium or rubidium iodide would show an even stronger response to X-rays (Section S10, Supporting Information), which would further improve its suitability as a cheap alternative to CR plates in nondestructive testing.

## 3. Conclusions

The full range of photochromic colors achievable in sodalites through simple substitutions and adjustments of the stoichiometry has been presented and its shortcomings discussed. This range has been expanded further by mixing easily synthesizable pink, yellow and blue photochromic sodalites together to produce robust materials capable of changing from white to orange, green, and brown. These could become attractive competitors to other inorganic materials showing these color changes which contain expensive and toxic elements, such as silver, fluorine and phosphorus.[8,23] This work represents another advance in the versatility of photochromic sodalites and has once again demonstrated how they can easily be commercialized for a huge range of everyday and specialist applications.

We have also shown how the activation threshold for F-center formation in photochromic sodalite can be reliably and incrementally lowered through gradual replacement of sulfur with selenium, without affecting the F-center's energy levels. The mechanistic origin of this effect is discussed along with the change in thermal bleaching energy. This effect remains consistent in sodalites with a variety of compositions and photochromism colors with minimal effect on the F-center's absorption spectrum. The drawbacks of selenium substitution are discussed, such as its tendency to affect the body color of the material. It is possible that a stronger reducing atmosphere will mitigate the issue of the darkening body color, as the $Se_2^-$ responsible for the color will get reduced to $Se_2^{2-}$. Such materials can be mixed with selenium-free sodalites of a contrasting color to produce a material capable of passively distinguishing between UVA, UVB and UVC radiation through the color it changes to upon exposure. We also demonstrated how spectroscopic analysis of the color change after simultaneous exposure to UVA and UVC can be used to quantify the doses of both.

Finally, we show how studies on how the composition affects the color reveal how these materials can be sensitized to X-ray radiation. Iodosodalite's blue color change produces images with significantly better contrast than chlorosodalite, is able to image dense inorganic samples in the dose ranges used in industry, and produces an equally clear image with less than half the dose required for chlorosodalite. Further testing with iodosodalites containing potassium and rubidium are expected to produce even better results.

## 4. Experimental Section

*Synthetic Procedures*: The majority of samples in this work were prepared from zeolite A in a solid-state method. The basic protocol involves grinding 0.700 g zeolite A (Sigma Aldrich) with 0.235 g NaCl (Sigma Aldrich, 99.5%) and 0.060 g $Na_2SO_4$ (E. Merck, 99%) by hand. This mixture is placed in an alumina boat and heated in air in a tube furnace to 850 °C for 5 h. Once the furnace had cooled, the mixture was ground again, placed in the same boat, and returned to a tube furnace, where it was heated again in a reducing atmosphere of 12% $H_2$/88% $N_2$ at 850 °C for 2 h. After the furnace had cooled, the sample was removed, in some cases washed with distilled water to remove soluble impurities, and characterized. NaCl was replaced with stoichiometric amounts of one or more other salts, such as LiCl (Acros, 99%), LiBr (Sigma Aldrich, 99%), LiI (Fluka Chemie, > 98%), NaBr (J. T. Baker), NaI (E. Merck), KCl (Merck, 99.5%), KBr (Merck), KI (Ega-Chemie, > 99%), RbCl (Merck), RbBr (Alfa Aesar, 99.8%), RbI (Sigma Aldrich, 99.9%), or $CaCl_2{\cdot}6H_2O$ (Riedel de Haën, 99%). In some cases, 0–100 mol% $Na_2SO_4$ was replaced with $Na_2SeO_3$ (Sigma Aldrich, 99%). Due to the toxicity and low decomposition temperature of $Na_2SeO_3$, these samples were prepared inside a quartz reactor with the furnace inside a fume hood.

Sodalites with the lowest energy absorption maxima in their colored forms (650–685 nm) were prepared using a hydrothermal method: 0.400 g $NaAlO_2$ (Sigma Aldrich), 0.240 g fumed $SiO_2$ (Sigma, 99.8%), 0.167 g $Na_2GeO_3$, 0.060 g $Na_2SO_4$, and 0.668 g KI were ground together by hand, then dissolved in a few mL of distilled water and transferred to a 23 mL Teflon cup that fitted in a small autoclave. The autoclave was sealed


© 2023 The Authors. Advanced Functional Materials published by Wiley-VCH GmbH

16163028, 0, Downloaded from https://onlinelibrary.wiley.com/doi/10.1002/adfm.202303398 by University of Turku, Wiley Online Library on [26/07/2023]. See the Terms and Conditions (https://onlinelibrary.wiley.com/terms-and-conditions) on Wiley Online Library for rules of use; OA articles are governed by the applicable Creative Commons License

and placed into an incubator at 180 °C for 48 h. After this stage, the resulting paste-like solution was transferred to an evaporating dish and placed in a drying oven (Termaks TS 8056) at 100 °C for 1–2 h to evaporate the remaining water. The resulting powder was collected, ground and transferred to an alumina boat. Samples were subsequently sintered in air at 850 °C for 5 h, and all samples were reduced in the same way as described above. Some of these materials were then subjected to potassium ion exchange to further red-shift their absorption maxima using the nitrate melt method as described by Johnson et al.[60] Sodalites of varying composition, prepared by solid-state and hydrothermal syntheses, were ground by hand with potassium nitrate (Alfa Aesar, 99%) in a 1:4 ratio by mass of sodalite to $KNO_3$. The mixture was transferred to an aluminum boat and heated in a tube furnace at 370 °C for 16 h. Once the product had cooled, it was washed with distilled water, centrifuged for 30 s and the liquid poured away. This was repeated four times.

The $Na_2GeO_3$ used above was prepared by grinding stoichiometric amounts of $Na_2CO_3$ (E. Merck, 99.5%) and $GeO_2$ (Sigma Aldrich, 99.99%) respectively and heating them at 800 °C for 48 h. The products were analyzed by powder X-ray diffraction (PXRD) and found to be pure.

Mixes showing different colors depending on excitation wavelength were prepared as follows: two sodalites were chosen based upon their measured tenebrescence excitation spectra such that one was excited by UVA or UVB and the other only by UVC. The two materials also had to have significantly different absorption maxima in their colored forms so that the two colors were distinguishable to both a spectrometer and the human eye. Once chosen, the two sodalites were mixed together in equal proportions with a pestle and mortar. Mixes showing new tenebrescence colors were prepared as follows: two or more sodalites were selected based on their observed tenebrescence colors, including the intensity of the absorption band. Samples with similar absorption intensities but at different wavelengths were selected and mixed together in equal proportions with a pestle and mortar. The resulting mixture was irradiated for 1 minute with 254 nm radiation to check the resulting color. More of a particular component was then added, if necessary, to adjust the color to that which was desired.

One sodalite mix was further mixed with an organic polymer matrix and cast into a thin flexible film. The tape casting method is based on that of Abhinay et al.[65] Sodalite (40 mass%), 2-butanone (30 mass%), ethanol (15 mass%), and Triton X-100 (2 mass%) were first mixed together in a Philips Minimill PW4018/00 ball mill at speed 1 for 10 min, after which polyvinyl butyral (7 mass%) and benzyl butyl phthalate (6 mass%) were added to the mixture, which was mixed in the same mill for 2 min at speed 5. The subsequent suspension was cast as a 350 µm coating onto a 0.1 mm thick Folex Premium Universal Copy Film X-100 A4 (art. no. 39 100.100.44000) polyethylene film using an Erichsen Coatmaster 510 applicator.

*Characterization Methods*: The presence of selenium was investigated with X-ray fluorescence spectroscopy (XRF) using a PANalytical Epsilon 1 device with internal Omnian calibration and a 50 kV Ag-anode X-ray tube with $K_\alpha$ emission at ≈22 keV. Results were compiled from four scans using a silver filter, a copper filter, an aluminum filter and no filter, respectively. Materials' structure and phase purity was assessed using powder X-ray diffraction performed with a Huber G670 detector and copper $K_{\alpha 1}$ radiation ($\lambda$ = 1.54060 Å). Exposure time was 30 min, with 10 readings of the imaging plate, or with a PANalytical Aeris benchtop instrument, with copper $K_{\alpha 12}$ radiation ( wavelength = 1.5406 Å ($K_{\alpha 1}$) and 1.5444 Å ($K_{\alpha 2}$)) with a step size of $2\theta = 0.011°$ and a measurement time of 29 min 45 s across the range 8–85° (more detail in Section S11, in the Supporting Information). Most materials showed only the desired sodalite phase, though small quantities of impurities such as $MAlSiO_4$ (M = K, Rb), MX (M = Na, K, Rb; X = Cl, Br), and nepheline ($Na_3KAl_4Si_4O_{16}$) were detected.

The change of color of the materials after UV irradiation was investigated using reflectance measurements under illumination of a 40 W incandescent lamp, with an incident irradiance of 1.34 W $m^{-2}$ in all measurements. The reflectance of the sample before excitation was measured and then used as the white background color. Occasionally MgO was used as a white reference to study the background color of the material. Samples were excited with 254 nm radiation from a UVP model UVLS-24 EL, 4 W 254/365 nm handheld lamp (UVC irradiance ≈3.0 mW $cm^{-2}$) for 5 min and their reflectance measured again 5 s after the lamp was switched off to show the change in reflectance. Spectra were collected using an Avantes FC-IR600-1-ME-HTX optical fibre connected to an Avantes HS-TEC CCD spectrometer with a data collection time of 1.6 s (160 ms integration time, 10 averages). The materials' colors were quantified as $L^*a^*b^*$ coordinates after 5 min irradiation with 254 nm from the 4 W handheld lamp using a Konica Minolta CM-2300d handheld spectrometer with its own white calibration disc.

Tenebrescence excitation spectra were recorded by irradiating the sample for 5 min with the following radiation wavelengths produced by a SB522 150 W Xe-arc lamp coupled to a LOT MSH 300 monochromator: 220, 240, 260, 280, 300, 325, 350, 375, and 400 nm. Fresh sample was used for each excitation wavelength. The reflectance of the sample was measured using the same HS-TEC spectrometer and optical fiber as previously mentioned under the illumination of a LS-1-CAL OceanOptics incandescent torch. The data collection time was 1.6 s (160 ms integration time, 10 averages). Reflectance was measured before irradiation and set as the white background; after irradiation reflectance was measured again. The reflectance wells were integrated to give the color intensity. Optical bleaching of tenebrescence was characterized by first measuring the sample's reflectance and setting this as the white reference. The sample was then excited with 260 nm radiation from the aforementioned LOT monochromator for 5 minutes and its reflectance measured. The sample was allowed to sit in darkness for a further 5 min, after which its reflectance was measured to obtain the spontaneous fading in darkness of the sample. The sample was subsequently recolored using 260 nm radiation for 5 min, then bleached with light ranging from 300 to 680 nm. The cycle was repeated using 20 nm steps in the bleaching wavelength. The reflectance wells were integrated to give color intensity, and the decrease in color intensity caused by each bleaching wavelength relative to the previous intensity after 260 nm excitation was calculated accounting for spontaneous fading in darkness. These results produced the optical bleaching spectra. Reflectance was measured using the same HS-TEC spectrometer, optical fiber, and OceanOptics incandescent torch as previously mentioned. The data collection time was 1.6 s (160 ms integration time, 10 averages).

Thermal bleaching energies were evaluated using thermotenebrescence.[27,41] The same optical fibre and HS-TEC spectrometer as mentioned previously were used, with a data collection time of 1 s (50 ms integration time, 20 averages). The sample's reflectance was measured before irradiation and used as the background. Similarly to before, the sample's reflectance was measured before irradiation as the white background, then measured again after 2 min of using a 254 nm handheld lamp as mentioned before (UVC irradiance ≈2.2 mW $cm^{-2}$). After coloration, the sample was then heated from 20 to 250 °C at a rate of 3 °C $s^{-1}$ using a MikroLab Thermoluminescent Materials Laboratory Reader RA'04. Using the data collection time of 1 s, a reflectance spectrum was acquired every second during the heating. The reflectance signal was corrected to account for the effects of heating on an uncolored sample, and then the curves were integrated to calculate the color intensity at each temperature. The color intensity values were also corrected for spontaneous fading under white light. Color intensity with respect to temperature was plotted to obtain the thermotenebrescence curve. Thermotenebrescence data was handled in a similar way to thermoluminescence data to calculate the depth of the trap involved in thermal bleaching. The curves were analyzed and the trap depths calculated using the initial rise method.[64]

Photos of other mixes showing two different tenebrescence colors after UVA and UVC excitation were produced by exciting the samples with the monochromator mentioned previously for 19 min (270 nm) or 13.2 min (325 nm). These times account for the relative emission intensity of the monochromator at those wavelengths and thus correspond to the same radiation dose.

Photoelectric absorption curves for photochromic sodalites of different compositions were calculated following the NIST X-ray Form Factor, Attenuation and Scattering tables using the formula $M_{20}Na_{60}Al_{60}Si_{60}O_{240}X_{18}S_1$, where M = Na, K, Rb and X = Cl, Br, I.[69] The stoichiometries of X and S used are based on those given by Williams


© 2023 The Authors. Advanced Functional Materials published by Wiley-VCH GmbH

16163028, 0, Downloaded from https://onlinelibrary.wiley.com/doi/10.1002/adfm.202303398 by University of Turku, Wiley Online Library on [26/07/2023]. See the Terms and Conditions (https://onlinelibrary.wiley.com/terms-and-conditions) on Wiley Online Library for rules of use; OA articles are governed by the applicable Creative Commons License

et al.[55] X-ray images of a dead flying ant and micro SD reader were taken by placing the subject in the aforementioned XRF device and a flexible tape prepared from the appropriate photochromic sodalite on top of it. The specimen was then irradiated for 26–61 min with the X-ray radiation by the XRF device to form the X-ray image. The tape was removed from the device and photographed. The rise of tenebrescence coloration with respect to X-ray dose was done by subjecting the film to the same radiation from the same device for 1–181 min, corresponding to doses of between 4–320 mSv. Doses were measured using a Thermo Scientific RadEye B20-ER. The reflectance of an uncolored portion of film was measured immediately after irradiation and set as the white reference. The reflectance of the colored region was then measured and the reflectance curve integrated to obtain the color intensity after that X-ray dose. Reflectance was measured using an Avantes AvaSpec-ULS2048CL-EVO CCD spectrometer coupled to an Avantes FC-UVIR600-1 optical fibre (integration time 200 ms, 10 averages), under illumination from a 40 W incandescent lamp at constant irradiance. The rise under UV was measured by exposing the tape to 254 nm UV radiation from the same lamp as previously mentioned for 15 s to 10 min at an incident irradiance of 4.4 mW $cm^2$. The change in reflectance was then measured in the same way as for the rise of coloration under X-ray described above.

*Computational Details*: All optimized structures obtained with the ab initio CRYSTAL17[73] code were conducted at the DFT/ PBE0[74] level of theory using localized basis sets. HF and KS equations were solved self-consistently with convergence criterion for the SCF cycles fixed at $10^{-7}$ Ha per unit cell. The reciprocal space was sampled according to a sublattice with a 12 × 12 × 12 k-points mesh for the geometry optimization of the bulk system, while a single k point (the Γ point) was used for the geometry optimization of the supercells. The basis set for the electron in the vacancy has been previously optimized and is of the form 111G(d).[56] All-electron double-$\zeta$ basis sets with polarization functions were used for Si ([4s3p1d]/(20s12p1d)),[75] Al ([4s3p1d]/(17s9p1d)),[76] O ([3s2p1d]/(10s4p1d)),[77] and Cl ([4s3p1d]/(16s10p1d)).[78] All-electron triple-$\zeta$ basis sets with polarization functions were used for Na ([4s3p1d]/(15s7p1d)[79] and S ([6s5p2d]/(20s14p2d)).[80] A pseudo potential was used for the 10 core electrons of selenium along with a ([5s4p2d]/(15s14p7d)) basis set for the 24 remaining electrons.

Spectroscopic investigations led on the extracted clusters (embedded in a sphere of pseudopotentials and an array of point charges),[56] were done at the TD-DFT/CAM-B3LYP level with the same basis set as the one used for periodic boundary condition calculations with Gaussian 16 package.[81]

## Supporting Information

Supporting Information is available from the Wiley Online Library or from the author.

## Acknowledgements

Thanks go to Sami Vuori for practical advice related to the X-ray imaging portion of the paper, to Dr. Pia Damlin for help with Raman spectroscopy, to Dr. Ian Pompermayer Machado for help obtaining the SEM images, and to Dr. Leonnam Merízio for proofreading the manuscript. The authors thank the following for financial support: the University of Turku Graduate School (UTUGS) Doctoral Programme in Exact Sciences (EXACTUS), the Turing Scheme of the UK Government, the emmy.network foundation under the aegis of the Fondation de Luxembourg, the SYSPROD project and AXELERA Pôle de Compétitivité (PSMN Data Center), and the French agency ANR (TeneMod project ANR-17-CE29-0007-21). This work was granted access to the HPC resources of CINES, IDRIS, and TGCC under the allocation 2018-080609 made by GENCI.

## Conflict of Interest

The authors declare no conflict of interest.

## Author Contributions

Hannah Byron – investigation, data curation, formal analysis, funding acquisition, writing – original draft, writing – review & editing. Claudia Swain – investigation, data curation, writing – review & editing. Pyry Paturi – formal analysis, writing – review & editing. Pauline Colinet – investigation, data curation, formal analysis, writing – review & editing. Raphaël Rullan – investigation, data curation, formal analysis. Vesa Halava – formal analysis, supervision, funding acquisition, writing – review & editing. Tangui Le Bahers – supervision, investigation, data curation, formal analysis, funding acquisition, writing – review and editing. Mika Lastusaari – conceptualization, funding acquisition, supervision, writing – review & editing. The manuscript was written through contributions of all authors. All authors have given approval to the final version of the manuscript.

## Data Availability Statement

The data that support the findings of this study are available from the corresponding author upon reasonable request.

## Keywords

dosimetry, imaging, photochromism, security markers, sodalite

Received: March 27, 2023
Revised: June 2, 2023
Published online:

[1] M. K. Purkait, M. K. Sinha, P. Mondal, R. Singh, in *Interface Science and Technology*, Vol. *25* (Eds: M. K. Purkait, M. K. Sinha, P. Mondal, R. Singh), Stimuli Responsive Polymeric Membranes, Elsevier, Amsterdam **2018**, pp. 115–144
[2] Z. Sekkat, W. Knoll, *Photoreactive Organic Thin Films*, Elsevier, Amsterdam **2002**.
[3] K. G. Yager, C. J. Barrett, in *Intelligent Materials*, Chapt. 17 (Eds: M. Shahinpoor, H.-J. Schneider), Azobenzene Polymers as Photomechanical and Multifunctional Smart Materials, The Royal Society of Chemistry, Cambridge **2007**, pp. 424–446, https://doi.org/10.1039/9781847558008-00424.
[4] A.-L. Leistner, Z. L. Pianowski, *Eur. J. Org. Chem.* **2022**, *2022*, e202101271.
[5] J. Zhang, Q. Zou, H. Tian, *Adv. Mater.* **2013**, *25*, 378.
[6] R. Pardo, M. Zayat, D. Levy, *Chem. Soc. Rev.* **2011**, *40*, 672.
[7] G. P. Smith, *J. Mater. Sci.* **1967**, *2*, 139.
[8] Y. Ohko, T. Tatsuma, T. Fujii, K. Naoi, C. Niwa, Y. Kubota, A. Fujishima, *Nat. Mater.* **2003**, *2*, 29.
[9] K. Naoi, Y. Ohko, T. Tatsuma, *J. Am. Chem. Soc.* **2004**, *126*, 3664.
[10] Y. Badour, V. Jubera, I. Andron, C. Frayret, M. Gaudon, *Opt. Mater.: X* **2021**, *12*, 100110.
[11] J. Wei, X. Jiao, T. Wang, D. Chen, *J. Mater. Chem. C* **2015**, *3*, 7597.
[12] A. Mukhopadhyay, J. N. Moorthy, *J. Photochem. Photobiol., C* **2016**, *29*, 73.
[13] S. Nishio, M. Kakihana, *Chem. Mater.* **2002**, *14*, 3730.
[14] S. S. Kanu, R. Binions, *Proc. Math. Phys. Eng. Sci.* **2010**, *466*, 19.
[15] X. Dong, Z. Wu, Y. Guo, Y. Tong, X. Liu, L. Zhang, Y. Lu, *Sol. Energy Mater. Sol. Cells* **2021**, *219*, 110784.
[16] C. Bechinger, E. Wirth, P. Leiderer, *Appl. Phys. Lett.* **1996**, *68*, 2834.
[17] H. Miyazaki, M. Inada, H. Suzuki, T. Ota, *J. Ceram. Soc. Jpn.* **2013**, *121*, 106.


© 2023 The Authors. Advanced Functional Materials published by Wiley-VCH GmbH

16163028, 0, Downloaded from https://onlinelibrary.wiley.com/doi/10.1002/adfm.202303398 by University of Turku, Wiley Online Library on [26/07/2023]. See the Terms and Conditions (https://onlinelibrary.wiley.com/terms-and-conditions) on Wiley Online Library for rules of use; OA articles are governed by the applicable Creative Commons License

[18] J. N. Schrauben, R. Hayoun, C. N. Valdez, M. Braten, L. Fridley, J. M. Mayer, *Science* **2012**, *336*, 1298.
[19] Y. Jin, Y. Lv, C. Wang, G. Ju, H. Wu, Y. Hu, *Sens. Actuators, B* **2017**, *245*, 256.
[20] Y. Lv, Y. Jin, C. Wang, L. Chen, G. Ju, Y. Hu, *RSC Adv.* **2017**, *7*, 43700.
[21] G. Ju, Y. Hu, L. Chen, X. Wang, *ECS Solid State Lett.* **2012**, *1*, R1.
[22] Y. Zhang, L. Luo, K. Li, W. Li, Y. Hou, *J. Phys. D: Appl. Phys.* **2018**, *51*, 365102.
[23] Y. Lv, Z. Li, Y. Jin, H. Wu, C. Wang, G. Ju, L. Chen, Z. Hu, Y. Hu, *Ceram. Int.* **2019**, *45*, 5971.
[24] Y. Lv, Y. Jin, C. Wang, G. Ju, F. Xue, Y. Hu, *J. Lumin.* **2017**, *186*, 238.
[25] Y. Jin, Y. Hu, Y. Fu, L. Chen, G. Ju, Z. Mu, *J. Mater. Chem. C* **2015**, *3*, 9435.
[26] Z. Yang, J. Du, L. I. D. J. Martin, D. Poelman, *J. Eur. Ceram. Soc.* **2021**, *41*, 1925.
[27] P. Colinet, H. Byron, S. Vuori, J.-P. Lehtiö, P. Laukkanen, L. Van Goethem, M. Lastusaari, T. Le Bahers, *Proc. Natl. Acad. Sci. USA* **2022**, *119*, e2202487119.
[28] J. A. Armstrong, M. T. Weller, *Dalton Trans.* **2006**, 2998, https://doi.org/10.1039/b600579a.
[29] S. F. McClure, G. R. Rossman, J. E. Shigley, *Gems Gemol.* **2005**, *41*, 269.
[30] International Mineralogical Association, *List of Minerals*, http://cnmnc.main.jp/IMA_Master_List_%282022-11%29.pdf (accessed: November 2022).
[31] D. B. Medved, *J. Chem. Phys.* **1953**, *21*, 1309.
[32] R. D. Kirk, *J. Electrochem. Soc.* **1954**, *101*, 461.
[33] R. D. Kirk, *Am. Mineral.* **1955**, *40*, 22.
[34] E. F. Williams, W. G. Hodgson, J. S. Brinen, *J. Am. Ceram. Soc.* **1969**, *52*, 139.
[35] W. Phillips, *J. Electrochem. Soc.* **1970**, *117*, 1557.
[36] C. Z. Doorn, D. J. Schipper, P. T. Bolwijn, *J. Electrochem. Soc.* **1972**, *119*, 85.
[37] I. F. Chang, *J. Electrochem. Soc.* **1974**, *121*, 815.
[38] T. Takeda, A. Watanabe, *J. Electrochem. Soc.* **1973**, *120*, 1414.
[39] L. T. Todd, A. Linz, E. F. Farrell, *IEEE Trans. Electron Devices* **1975**, *22*, 788.
[40] I. Norrbo, J. M. Carvalho, P. Laukkanen, J. Mäkelä, F. Mamedov, M. Peurla, H. Helminen, S. Pihlasalo, H. Härmä, J. Sinkkonen, M. Lastusaari, *Adv. Funct. Mater.* **2017**, *27*, 1606547.
[41] I. Norrbo, A. Curutchet, A. Kuusisto, J. Mäkelä, P. Laukkanen, P. Paturi, T. Laihinen, J. Sinkkonen, E. Wetterskog, F. Mamedov, T. Le Bahers, M. Lastusaari, *Mater. Horiz.* **2018**, *5*, 569.
[42] S. Vuori, P. Colinet, I. Norrbo, R. Steininger, T. Saarinen, H. Palonen, P. Paturi, L. C. V. Rodrigues, J. Göttlicher, T. Le Bahers, M. Lastusaari, *Adv. Opt. Mater.* **2021**, *9*, 2100762.
[43] S. Vuori, P. Colinet, J.-P. Lehtiö, A. Lemiere, I. Norrbo, M. Granström, J. Konu, G. Ågren, P. Laukkanen, L. Petit, A. J. Airaksinen, L. Goethem, T. L. Bahers, M. Lastusaari, *Mater. Horiz.* **2022**, *9*, 2773.
[44] S. Vuori, H. Byron, I. Norrbo, M. Tuomisto, M. Lastusaari, *J Ind Eng Chem* **2023**, *120*, 361.
[45] I. Norrbo, P. Gluchowski, P. Paturi, J. Sinkkonen, M. Lastusaari, *Inorg. Chem.* **2015**, *54*, 7717.
[46] H. Byron, T. Kreivilä, P. Colinet, T. L. Bahers, M. Lastusaari, *J. Mater. Chem. C* **2023**, *11*, 3360.
[47] G. Hoffmann, *GMS Krankenhhyg Interdiszip* **2007**, *2*, Doc54.
[48] C. Agamah, S. Vuori, P. Colinet, I. Norrbo, J. M. de Carvalho, L. K. Okada Nakamura, J. Lindblom, L. van Goethem, A. Emmermann, T. Saarinen, T. Laihinen, E. Laakkonen, J. Lindén, J. Konu, H. Vrielinck, D. Van der Heggen, P. F. Smet, T. L. Bahers, M. Lastusaari, *Chem. Mater.* **2020**, *32*, 8895.
[49] I. Norrbo, P. Gluchowski, I. Hyppänen, T. Laihinen, P. Laukkanen, J. Mäkelä, F. Mamedov, H. S. Santos, J. Sinkkonen, M. Tuomisto, A. Viinikanoja, M. Lastusaari, *ACS Appl. Mater. Interfaces* **2016**, *8*, 11592.
[50] P. Colinet, T. L. Bahers, *J. Mater. Chem. C* **2023**, *11*, 730.
[51] P. Colinet, Tenebrescent Minerals by in Silico Modelling. These de doctorat, Lyon, **2022**, https://www.theses.fr/2022LYSEN002 (accessed: October 2022).
[52] D. W. G. Ballentyne, K. L. Bye, *J. Phys. D: Appl. Phys.* **1970**, *3*, 1438.
[53] D. Reinen, G.-G. Lindner, *Chem. Soc. Rev.* **1999**, *28*, 75.
[54] Nuclear Physics Experience http://nupex.eu/index.php?g=textcontent/nuclearapplications/xraymed%lang=en (accessed: February 2023).
[55] E. R. Williams, A. Simmonds, J. A. Armstrong, M. T. Weller, *J. Mater. Chem.* **2010**, *20*, 10883.
[56] P. Colinet, A. Gheeraert, A. Curutchet, T. Le Bahers, *J. Phys. Chem. C* **2020**, *124*, 8949.
[57] G. M. Johnson, Synthesis and Characterisation of Aluminosilicate and Framework Modified Sodalites¸ *Ph.D. Thesis*, University of Southampton, Faculty of Science, Department of Chemistry, **1996**.
[58] R. Radler, *Inorganic Phototropic Materials for High Density Computer Memories*, Defense Technical Information Center, Fort Belvoir, VA **1963**.
[59] *The Periodic Table of Endangered Elements*, American Chemical Society, https://www.acs.org/greenchemistry/research-innovation/endangered-elements.html (accessed: December 2022).
[60] G. M. Johnson, P. J. Mead, M. T. Weller, *Microporous Mesoporous Mater.* **2000**, *38*, 445.
[61] I. Norrbo, I. Hyppänen, M. Lastusaari, *J. Lumin.* **2017**, *191*, 28.
[62] H. Schlaich, G.-G. Lindner, J. Feldmann, E. O. Göbel, D. Reinen, *Inorg. Chem.* **2000**, *39*, 2740.
[63] R. J. H. Clark, T. J. Dines, M. Kurmoo, *Inorg. Chem.* **1983**, *22*, 2766,.
[64] F. J. Garlick, F. Gibson, *Proc. Phys. Soc.* **1948**, *60*, 574.
[65] S. Abhinay, R. Mazumder, A. Seal, A. Sen, *J. Eur. Ceram. Soc.* **2016**, *36*, 3125.
[66] T. S. Curry, J. E. Dowdey, R. C. Murry, *Christensen's Physics of Diagnostic Radiology*, Lippincott Williams & Wilkins, Philadelphia, PA **1990**.
[67] I. Szalóki, T. Pintér, I. Szalóki, G. Radócz, A. Gerényi, *J. Anal. At. Spectrom.* **2019**, *34*, 1652.
[68] *Mini-X2 X-Ray Tube System for XRF – Amptek – X-Ray Detectors and Electronics*, https://www.amptek.com/products/mini-x2-x-ray-tube (accessed: February 2023).
[69] C. T. Chantler, K. Olsen, R. A. Dragoset, J. Chang, A. R. Kishore, S. A. Kotochigova, D. S. Zucker, NIST X-Ray Form Factor, Attenuation and Scattering Tables (Version 2.1), https://physics.nist.gov/PhysRefData/FFast/html/form.html (accessed: January 2023).
[70] GE Inspection Technologies, *Industrial Radiography: Image Forming Techniques*, Pennsylvania, USA **2008**.
[71] R. D. Deslattes, E. G. Kessler Jr., P. Indelicato, L. de Billy, E. Lindroth, J. Anton, J. S. Coursey, D. J. Schwab, C. Chang, R. Sukumar, K. Olsen, R. A. Dragoset, *X-Ray Transition Energies Database (Version 1.2)*, NIST, https://www.nist.gov/pml/x-ray-transition-energies-database (accessed: February 2023).
[72] R. Behling, *Modern Diagnostic X-Ray Sources: Technology, Manufacturing, Reliability*, Vol. *2*, Ringgold Inc, Beaverton, USA **2015**.
[73] R. Dovesi, V. R. Saunders, C. Roetti, R. Orlando, C. M. Zicovich-Wilson, F. Pascale, B. Civalleri, K. Doll, N. M. Harrison, I. J. Bush, P. D'Arco, M. Llunell, M. Causà, Y. Noël, L. Maschio, A. Erba, M. Rerat, S. Casassa, CRYSTAL17, **2017**.
[74] C. Adamo, V. Barone, *J. Chem. Phys.* **1999**, *110*, 6158.
[75] R. Nada, J. B. Nicholas, M. I. McCarthy, A. C. Hess, *Int. J. Quantum Chem.* **1996**, *60*, 809
[76] R. Demichelis, Y. Noel, B. Civalleri, C. Roetti, M. Ferrero, R. Dovesi, *J. Phys. Chem. B* **2007**, *111*, 9337.


© 2023 The Authors. Advanced Functional Materials published by Wiley-VCH GmbH

16163028, 0, Downloaded from https://onlinelibrary.wiley.com/doi/10.1002/adfm.202303398 by University of Turku, Wiley Online Library on [26/07/2023]. See the Terms and Conditions (https://onlinelibrary.wiley.com/terms-and-conditions) on Wiley Online Library for rules of use; OA articles are governed by the applicable Creative Commons License

[77] M. Corno, C. Busco, B. Civalleri, P. Ugliengo, *Phys. Chem. Chem. Phys.* **2006**, *8*, 2464.
[78] P. C. Hariharan, J. A. Pople, *Theoret. Chim. Acta* **1973**, *28*, 213.
[79] G. Sophia, P. Baranek, C. Sarrazin, M. Rerat, R. Dovesi, www.crystal.unito.it/Basis_Sets/sodium.html (accessed: February 2023).
[80] D. Vilela Oliveira, J. Laun, M. F. Peintinger, T. Bredow, *J. Comput. Chem.* **2019**, *40*, 2364.
[81] M. J. Frisch, G. W. Trucks, H. B. Schlegel, G. E. Scuseria, M. A. Robb, J. R. Cheeseman, G. Scalmani, V. Barone, G. A. Petersson, H. Nakatsuji, X. Li, M. Caricato, A. V. Marenich, J. Bloino, B. G. Janesko, R. Gomperts, B. Mennucci, H. P. Hratchian, J. V. Ortiz, A. F. Izmaylov, J. L. Sonnenberg, D. Williams-Young, F. Ding, F. Lipparini, F. Egidi, J. Goings, B. Peng, A. Petrone, T. Henderson, et al., Gaussian 16 Revision C.01, **2016**.


© 2023 The Authors. Advanced Functional Materials published by Wiley-VCH GmbH

16163028, 0, Downloaded from https://onlinelibrary.wiley.com/doi/10.1002/adfm.202303398 by University of Turku, Wiley Online Library on [26/07/2023]. See the Terms and Conditions (https://onlinelibrary.wiley.com/terms-and-conditions) on Wiley Online Library for rules of use; OA articles are governed by the applicable Creative Commons License